Peer-reviewed version available at C 2018, 4, 39; doi:10.3390/c4030039

Article

CUBIT: Capacitive qUantum BIT

Sina Khorasani [1]

[1] Vienna Center for Quantum Science and Technology, University of Vienna, 1090 Vienna, Austria ; sina.khorasani@gmail.com

Abstract: In this letter, it is proposed that cryogenic quantum bits could operate based on the nonlinearity due to the quantum capacitance of two-dimensional Dirac materials, and in particular graphene. The anharmonicity of a typical superconducting quantum bit is calculated and the sensitivity of quantum bit frequency and anharmonicty with respect to temperature are found. Reasonable estimates reveal that a careful fabrication process could reveal the expected properties, thus putting the context of quantum computing hardware into new perspectives.

Keywords: Graphene, Two-dimensional Materials, Nonlinear Quantum Circuits, Quantum Bits

1. Introduction

We discuss a new type of qubit with integrability, based on a nonlinear Quantum Capacitor (QC) made of the two-dimensional materials [1], Graphene (Gr) and Boron Nitride (BN). Without exception, all existing superconducting qubits [2–4] rely on the nonlinear inductance of Josephson Junctions (JJs). Here, the nonlinear inductance is replaced by the nonlinear capacitance coming from two Gr monolayers separated by a multilayer BN, which acts as a potential barrier and forms a parallel plate capacitance [1].

The nonlinearity of such a quantum capacitor stems from the two-dimensionality of crystal combined with the Dirac cone in its band structure, where a square-root correspondence between the Fermi energy E_F and external voltage V is established. There is no fundamental reason why other 2D Dirac materials, such as Silicene and Germanene [5–8] could not be used for this purpose.

On the practical side, two major obstacles seem to influence the design. One is the compatibility of Gr with superconducting circuits, and the next one is the potential puddles arising from crystal imperfections and impurities. Recent progress on large scale and near-perfect crystalline growth of Gr [9], which is equally applicable to BN, should in principle resolve the issues tied to the puddles to a great extent. Also, recent discoveries on the existence of p-wave induced phase of superconductivity in Gr [10] as well as unconventional superconducting phase of twisted bilayer Gr at the magic angle of 19.19mRad [11] rises hopes for practicality of such a design. The latter, offers a large decrease of Fermi velocity at the vicinity of Dirac cone, which helps in a significant reduction in qubit size as well as relaxation of stringing limits imposed by the fabrication technology.

It is the purpose of this letter to establish the feasibility of *CUBIT*, which we use to refer to the nonlinear Capacitive qUantum BIT. While we present the numerical design of a preliminary CUBIT, the fundamental aspects and practicality issues which are involved are also discussed. Another potentially useful application of nonlinear quantum capacitance could be in the cryogenic quantum-limited parametric amplifiers.

2. Results

This sandwich structure shown in Fig. 1 is routinely used owing to its peculiar electronic and optical properties [12,13]. Quite interestingly, its application to a quantum-dot charge qubit design has been also demonstrated [14], which is however incompatible with the conventional superconducting quantum circuits.

For the BN thickness of 3nm to 70nm, the contribution of geometric parallel plate capacitance of the structure has been shown that can be neglected [2], and the quantum capacitance is given by

$$C_Q = \frac{2e^2 \ln(16) S k_B T}{\pi(\hbar v_F)^2} \ln\left[\frac{1}{8}\left(1 + \cosh\frac{E_F}{k_B T}\right)\right], \quad (1)$$

where v_F is the Fermi velocity of graphene, k_B is the Boltzmann's constant, e is the electronic charge, S is the total geometric 2D area of capacitor, and T is the absolute temperature. Evidently, the quantum capacitance is nonlinear since it depends on the applied voltage $V = 2E_F/e$.

The recently discovered superconductivity in twisted bilayer Gr at the magic angle [11], offers a roughly 7-fold reduction in v_F. This can cause a significant reduction of the necessary capacitance area up to a factor of roughly 50, since $C_Q \propto S/v_F^2$, while maintaining the same level of anharmonicity A. However, such a structure needs voltage bias and also cannot accommodate a large number of carriers. That would necessitate a serious look and separate study.

The bulk of the proposed qubit is a nonlinear anharmonic oscillator, which forbids transitioning from $|0\rangle$ to $|n\rangle\,; n > 1$ states with a given fixed pump. This has been schematically shown in Fig. 2. Signal can be fed into the oscillator by inductive coupling, or capacitive coupling similar to the qubits based on Josephson junctions [4,15]. The strength of anharmonicity could be adjusted by temperature as well as other available design parameters of the layered capacitor.

The total linear and nonlinear part of the QC can be then expanded as power series in terms of the applied voltage. By placing a linear inductor is across the QC, the total Hamiltonian up to fifth order is found, with remarkably large anharmonicity A. It is possible to tweak the design flexibility by placing a shunt linear capacitor across the QC. It is found that A rapidly increases with the temperature decreasing and also is a strong function of the capacitance area [1], and at temperatures of a few 0.1K easily yield strong nonlinearity. Signal can be fed into the qubit oscillator by inductive or capacitive coupling similar to the qubits based on JJs [2].

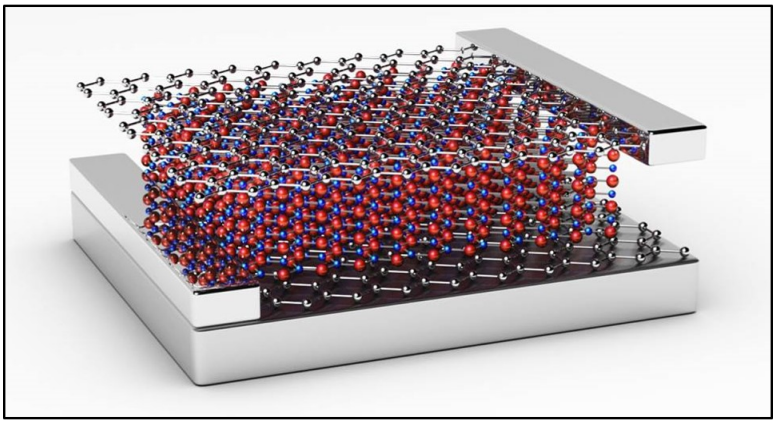

Figure 1. Graphene/Boron Nitride/Graphene sandwitch structure. Wide aluminum contacts are attached across the edges.

It is possible to tweak the design flexibility by placing the linear capacitors C_S and C_P respectively in series and across the quantum capacitor as shown in Fig. 2 in green color. This placement of the shunt capacitor C_P also could relax the restriction on the maximum operation temperature given as $\hbar\omega > 2k_B T$. It should be noticed that the existence of extra capacitors decrease the large anharmonicity delivered by the quantum capacitance C_Q.

Shown in Fig. 3, it is furthermore possible to combine the QC with JJs, where A is caused by the combined effects of JJ and QC. Quite clearly, the resonance frequency of the circuit is now also dependent on linear inductance of the JJ as well. A proper design can cause complete cancellation

of or enhancement in the anharmonicity of A, leaving nonlinear terms of sixth and higher orders. Furthermore, positive or negative A become now both accessible, using appropriate biasing of the JJs.

The combined effects of such an anharmonic oscillator can be expressed by the Hamiltonian

$$\mathbb{H} = \hbar\omega\left(\hat{a}^{\dagger}\hat{a} + \frac{1}{2}\right) + \frac{1}{4}\hbar\omega(\alpha - \omega\tau)\left(\hat{a}^{\dagger} + \hat{a}\right)^{4}, \tag{2}$$

where α is the contribution of JJs, and τ is the characteristic time of nonlinear interaction for the quantum capacitor [2]. This value has been already estimated theoretically [2] for a weakly nonlinear regime, which is not obviously a matter of interest in qubit design. The reason is that the anharmonicity should be actually large to guarantee two-level operation of the oscillator, strictly allowing no more than 1 photon at the qubit frequency ω to survive in the oscillator. Therefore, in this study τ has been numerically estimated by accurate solution of the nonlinear Hamiltonian potential, and obtaining the energy eigenvalue levels. Energy eigenvalues are found using a recent semi-analytical method reported elsewhere [16], which is at least as reliable as WKB but much easier to implement.

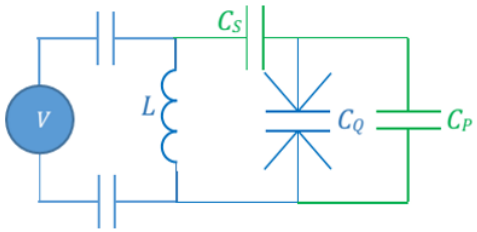

Figure 2. Illustration of the basic capacitive quantum bit design. The addition of series and parallel extra capacitors adds up to the design flexibility.

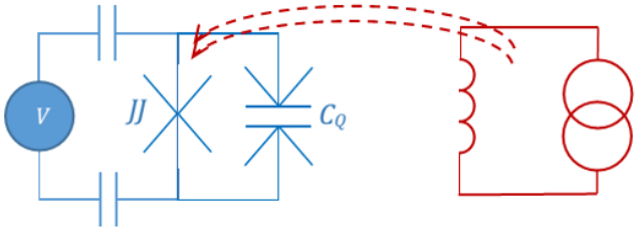

Figure 3. Illustration of a combined nonlinear quantum capacitance and Josephson-Junction design.

Since the structure has to be operated inside a dilution refrigerator with some temperature instability and drift over time, and the fact that the quantum capacitance is a function of temperature, one should make an estimate of qubit frequency $\omega = 2\pi f$ variations with temperature.

Also, the proposed qubit as an anharmonic oscillator, is also dependent on the graphene area as well. One may put the nonlinear Hamiltonian of the whole qubit together and solve for the eigenstates, which correspondingly yield the energy eigenvalues and therefore the anharmonicity. A typical dependence of the potential energy of the anharmonic circuit, including contributions of the quantum and series capacitance looks like the following in Fig. 4.

Since the oscillator is strongly anharmonic, the ultimate actual transition frequency can be different from the initial value by design. This anharmonicity is not only a function of temperature, but also a function of capacitor area, too. This dependence has been investigated as follows in Fig. 5.

The largest available range of anharmonicity occurs at the capacitor area of the order of $5 \times 10^4 \mu\text{m}^2$ to $10^5 \mu\text{m}^2$. Hence, a desirable capacitor size could be chosen to be around $50\mu\text{m} \times 1\text{mm}$, which together an inductor of 60nH would yield a qubit frequency of $\omega = 2\pi \times 3.55\text{GHz}$. This area is evidently small enough to be considered for easy fabrication and also integration. The temperature sensitivity could be

Preprints (www.preprints.org) | NOT PEER-REVIEWED | Posted: 15 May 2018 doi:10.20944/preprints201805.0201.v1

Peer-reviewed version available at C 2018, 4, 39; doi:10.3390/c4030039

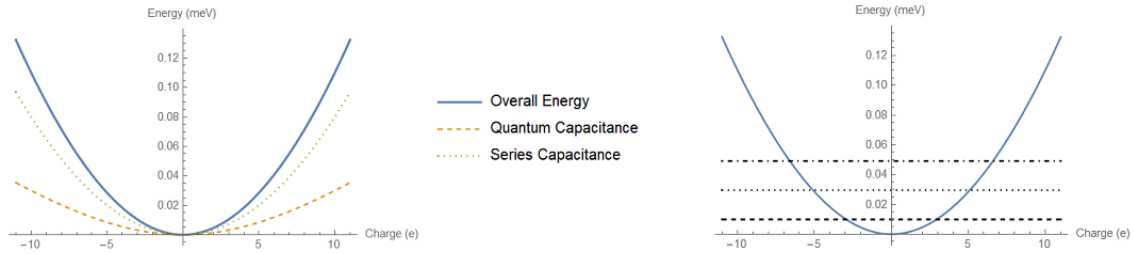

Figure 4. Calculation of energy levels of the anharmonic oscillator composed of nonlinear quantum capacitor and linear inductor showin in Fig. 2.

observed by inspection of the temperature-dependent variations of qubit frequency. This is illustrated in the Fig. 6.

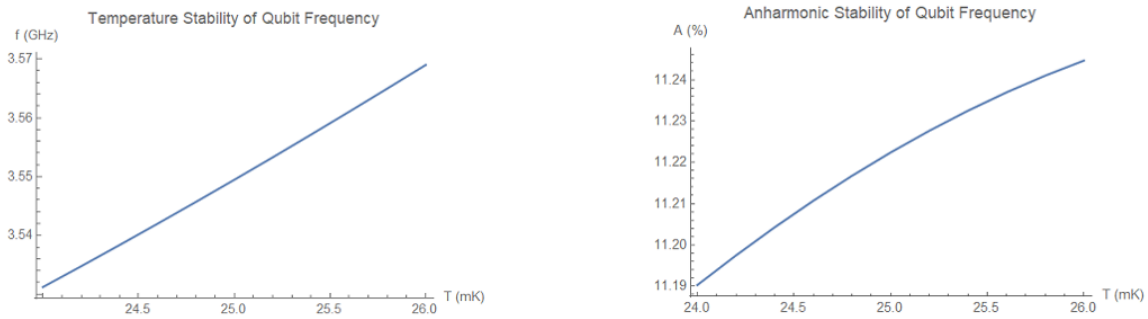

Figure 5. Variations of qubit frequency and anharmonicity versus operation temperature of the dilution fridge.

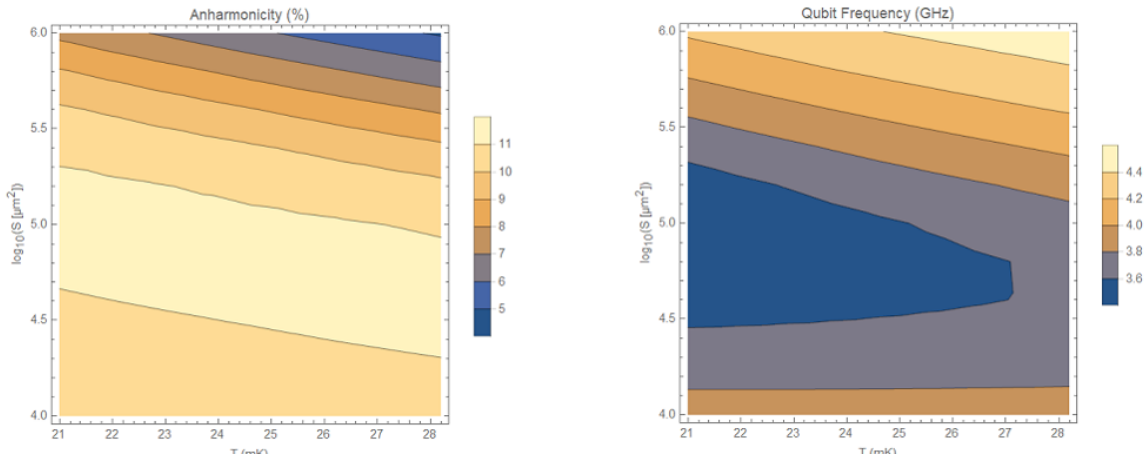

Figure 6. Contour plots of anharmonicity and qubit frequency versus temperature and qubit area.

This calculation gives the estimates of

$$\begin{aligned} \frac{\partial f}{\partial T} &= 19 \frac{\text{MHz}}{\text{mK}}, \\ \frac{\partial A}{\partial T} &= 0.027 \frac{\%}{\text{mK}}, \end{aligned} \tag{3}$$

which at an operation temperature of 25mK are equivalent to the operational sensitivities of

$$\begin{aligned} S_f^T &= \frac{\partial f/f}{\partial T/T} \times 100\% = 9.5\%, \\ S_A^T &= \frac{\partial A/A}{\partial T/T} \times 100\% = 6.1\%. \end{aligned} \tag{4}$$

Some design numbers are shown in Table 1, while redesigning with a series capacitor of 0.1pF to 1pF gives the data in Table 2.

Table 1. Qubit designs with no series capacitor $S = 1\text{mm}^2$.

S (mm^2)	Design $\omega/2\pi$ (GHz)	T (mK)	C_S (fF)	Actual $\omega/2\pi$ (GHz)	A (%)
1	2.5	25	–	2.29	3.9
1	5	25	–	4.41	6.04
1	10	25	–	8.31	8.26

Table 2. Qubit designs with a series capacitor $S = 1\text{mm}^2$.

S (mm^2)	Design $\omega/2\pi$ (GHz)	T (mK)	C_S (fF)	Actual $\omega/2\pi$ (GHz)	A (%)
1	2.5	25	100	2.39	0.44
1	5	25	100	4.77	0.76
1	10	25	1000	8.71	5.67

No surprise that the presence of the series capacitor should cause a reduction in anharmonicity A, since it makes the capacitive behavior of the whole circuit more linear. In general, increasing the frequency, while reducing the capacitor area seems to lead into an even more desirable set of numbers shown in Table 3.

Table 3. Qubit designs with no series capacitor $S = 0.1\text{mm}^2$.

S (mm^2)	Design $\omega/2\pi$ (GHz)	T (mK)	C_S (fF)	Actual $\omega/2\pi$ (GHz)	A (%)
0.1	10	25	–	6.42	11.2
0.1	15	25	–	11.1	9.02
0.1	20	25	–	11.5	11.1

Here, we ultimately choose the capacitor area of $S = 5 \times 10^4 \mu\text{m}^2$ which is 50μm wide and 1mm long, together with an inductor of $L = 60\text{nH}$, which yields the qubit frequency of $\omega = 2\pi \times 3.55\text{GHz}$, and anharmonicity of $A = 11\%$. The zero-point voltage and carrier number at the qubit frequency is estimated to be around $V_{\text{zp}} = 15\mu\text{V}$ and $n_{\text{zp}} = 1.7$. All contacts and connecting materials can be chosen to be Aluminum, since not only it easily superconducts at the temperatures of interest, but also, is a quite typical metal of choice in superconducting qubits.

It has to be mentioned again that employing the superconducting bilayer graphene [11] can in principle cause up to a 50-fold reduction in qubit area. That would limit the typical qubit area only to $S = 10^3 \mu\text{m}^2$, which is now a highly reasonable value.

3. Practical Considerations

3.1. Potential Puddles

In graphene, non-ideal impurities and defects at the interface do exist. Although their density can be minimized by exfoliation under high-vacuum and also encapsulations with 2D hexagonal BN, they persist to certain densities. Traps form shallow potential kinks, named as puddles.

Puddles are expected to be frozen and unmoving at ultralow temperatures. But their density and potential depth can be a matter of concern. For the quantum capacitance of Gr to survive, it is

estimated that the puddle surface density must be under $N_{\rm pd} < 10^8 {\rm cm}^{-2}$, which is roughly 1 defect per every 10^8 Carbon atom in Gr lattice. Furthermore, puddle potential energy depth must be bounded by $U_{\rm pd} < 10$meV. Values exceeding these bounds are undesirable and result in destroying the quantum capacitance property of Gr.

Typical values which are achieved in the experiments are not better than $10^10 {\rm cm}^{-2}$ yet. While this might seem a bit disappointing, the recent remarkable progress in very large-scale crystalline CVD growth of Gr and two-dimensional materials [9], highlights the likelihood of this possiblity, and even much better values to be attained soon.

The superconducting twisted bilayer graphene at the magic angle [11], not only could result in significant reduction of qubit size, but also may largely relax the constraints on the puddle density. This can be studied in depth either by ab-initio approaches such as the Density Function Theory, or through a series of carefully conducted experiments.

3.2. Zero-point Fluctuations

With regard to the effect of impurity charges, these appear as a background bias in the overall charge density. For a designed device to be practically useful at the single photon level, the zero-point charge fluctuations should exceed the impurity charges. The correct way to obtain zero-point amplitudes is to look for the corresponding values which reproduce the energy of half-quanta $\frac{1}{2}\hbar\omega$.

3.3. Decoherence and Dephasing

Possible mechanisms for qubit decoherence and dephasing may be considered, which include but are not limited to spontaneous emission from excited states, enhancement of emission rate due to the Purcell enhancement (when the qubit is placed inside a high-Q microwave cavity), substrate dielectric losses, nonideal proximity effects of carrier transport in graphene, tunneling across the dielectric due to defects and periphery surface states, coupling to spurious modes and surface acoustic waves, charge noise, flux noise, strain noise (which cause fluctuations and anisotropy in the Fermi velocity v_F).

Few of these have already been studied for transmon qubits [4,15], and their practical limits have been evaluated. Some have to be studied in great details which needs a deep theoretical study. It should be pointed out that there exists a very recent $0-\pi$ qubit design strategy [17], which offers inherent immunity with respect to decoherence. While this has to be tested experimentally yet, a topological dual of this strategy may in principle be applied to the anharmonic CUBIT under consideration here as well.

One has to keep in mind that superconducting qubits have already come a long way over the past 18 years, with their coherence times being initially only around 1ns [4]. Meanwhile the coherence performance of transmons is now for all practical reasons being saturated to 0.1ms for the best available designs and fabrication processes, such as the one being used in IBM-Q. That would be already a 10^5 fold improvement.

3.4. Parametric Amplifiers

An alternative potential use for this type of non-dissipative cryogenic nonlinear element could be in parametric amplifiers, which are of rather high importance in quantum science and technology. This can happen even if the qubit design criteria cannot be satisfied. The existing parametric amplifiers mostly are based on either Josephson-Junctions held at the same temperature of cryostat, or High-Electron Mobility Transistors (HEMTs) made of III-V semiconductor heterostructures, held typically at the operation temperature of 4K, much above the temperature of dilution fridge. Besides added noise as a result of higher-operation temperatures, usage of HEMTs will just increases the complexity of circuit designs and interfacing. Existence of nonlinear quantum capacitors can offer added flexibility and convenience to this particular application.

4. Conclusions

The Graphene/Boron Nitride/Graphene sandwich structure seems to be promising for quantum bit applications, where the nonlinearity of quantum capacitance replaces the nonlinearity of Josephson junctions. This should significantly alleviate the problem of cross-talk and altogether remove the qubit decoherence due to interference with stray magnetic fields. Using the bilayer graphene at the magic angle could be a game changer, however, the effects of potential puddles needs careful study. Probably, only experiments will be decisive that whether such sandwich structures could envision prospects of new qubits with enhanced decoherence and dephasing properties.

Acknowledgments: Discussions of this work with Dr. Sungkun Hong at Universität Wien is highly appreciated. A preliminary version of this study was presented at the Frontiers of Cricuit QED and Optomechanics which was held on February 12-14, 2018 at *Institute of Science and Technology*, Klosterneuburg, Austria.

Conflicts of Interest: The author declares no competing or conflict of interest.

References

1. Xia, J.; Chen, F.; Li, J.; Tao, N. Measurement of the quantum capacitance of graphene. *Nat. Nanotech.* **2009**, *4*, 505.
2. Khorasani, S.; Koottandavida, A. Nonlinear graphene quantum capacitors for electro-optics. *npj 2D Mat. Appl.* **2017**, *1*, 7.
3. Humble, T.S.; Thapliyal, H.; Muñoz-Coreas, E.; Mohiyaddin, F.A.; Bennink, R.S. Quantum computing circuits and devices. *arXiv* **2018**, 1804.10648.
4. Wendin, G. Quantum information processing with superconducting circuits: A review. *Rep. Prog. Phys.* **2017**, *80*, 106001.
5. Wu, H.; Qian, Y.; Du, Z.; Zhu, R.; Kan, E.; Deng, K. Prediction of another semimetallic silicene allotrope with Dirac fermions. *Phys. Lett. A* **2017**, *381*, 3754.
6. Acun, A.; Zhang, L.; Bampoulis, P.; Farmanbar, M.; van Houselt, A.; Rudenko, A.N.; Lingenfelder, M.; Brocks, G.; Poelsema, B.; Katsnelson, M. I. Germanene: the germanium analogue of graphene. *J. Phys.: Condens. Matter* **2015**, *27*, 443002.
7. Wang, J.; Deng, S.; Liu, Z.; Liu, Z. The rare two-dimensional materials with Dirac cones. *Nat. Sci. Rev.* **2015**, *2*, 22.
8. Balendhran, S.; Walia, S.; Nili, H.; Sriram, S.; Bhaskaran, M. Elemental analogues of Graphene: Silicene, Germanene, Stanene, and Phosphorene. *Small* **2014**, *11*, 640.
9. Vlassiouk, I.V.; Stehle, Y.; Pudasaini, P.R.; Unocic, R.R.; Rack, P.D.; Baddorf, A.P.; Ivanov, I.N.; Lavrik, N.V.; List, F.; Gupta, N.; Bets, K.V.; Yakobson, B.I.; Smirnov, S.N. Evolutionary selection growth of two-dimensional materials on polycrystalline substrates. *Nat. Mater.* **2018**, *17*, 318.
10. Di Bernardo, A.; Millo, O.; Barbone, M.; Alpern, H.; Kalcheim, Y.; Sassi, U.; Ott, A.K.; De Fazio, D.; Yoon, D.; Amado, M.; Ferrari, A.C.; Linder, J.; Robinson, J.W.A. p-wave triggered superconductivity in single-layer graphene on an electron-doped oxide superconductor. *Nat. Commun.* **2017**, *8*, 14024.
11. Cao, Y.; Fatemi, V.; Fang, S.; Watanabe, K.; Taniguchi, T.; Kaxiras, E.; Jarillo-Herrero, P. Unconventional superconductivity in magic-angle graphene superlattices. *Nature* **2018**, *556*, 43.
12. Khorasani, S. Tunable spontaneous emission from layered graphene/dielectric tunnel junctions. *IEEE J. Quant. Electron.* **2014**, *50*, 307.
13. Ranjan, V.; Zihlmann, S.; Makk, P.; Watanabe, K.; Taniguchi, T.; Schönenberger, C. Contactless microwave characterization of encapsulated graphene p-n junctions. *Phys. Rev. Appl.* **2017**, *7*, 054015.
14. Freitag, N.M.; Reisch, T.; Chizhova, L.A.; Nemes-Incze, P.; Holl, C.; Woods, C.R.; Gorbachev, R.V.; Cao, Y.; Geim, A.K.; Novoselov, K.S.; Burgdörfer, J.; Libisch, F.; Morgenstern, M. Large tunable valley splitting in edge-free graphene quantum dots on boron nitride. *Nat. Nanotech.* **2018**, doi:10.1038/s41565-018-0080-8.
15. Koch, J.; Yu, T.M.; Gambetta, J.; Houck, A.A.; Schuster, D.I.; Majer, J.; Blais, A.; Devoret, M.H.; Girvin, S.M.; Schoelkopf, R.J. Charge-insensitive qubit design derived from the Cooper pair box. *Phys. Rev. A* **2007**, *76*, 042319.
16. Khorasani, S. New basis functions for wave equation. *Scientia Iranica* **2016**, *23*, 2928.

17. Groszkowski, P.; Di Paolo, A.; Grimsmo, A.L.; Blais, A.; Schuster, D.I.; Houck, A.A.; Koch, J. Coherence properties of the $0-\pi$ qubit. *arXiv* **2017**, 1708.02886.